Anti-aging Effects of Alu Antisense RNA on Human Fibroblast Senescence Through the MEK-ERK Pathway Mediated by KIF15*

Ning JI[1], Chong-guang WU[1], Xiao-die WANG[1], Zhi-xue SONG[1], Pei-yuan WU[1], Xin LIU[1], Xu FENG[1], Xiang-mei ZHANG[2], Xiu-fang WANG[1#], Zhan-jun LV[1#]
[1]*Department of Genetics, Hebei Medical University, Hebei Key Lab of Laboratory Animal, Shijiazhuang 050017, China*
[2]*Research Center, Fourth Hospital of Hebei Medical University, Shijiazhuang 050011, China*

© Huazhong University of Science and Technology 2023

[Abstract] Objective: To investigate whether human short interspersed nuclear element antisense RNA (Alu antisense RNA; Alu asRNA) could delay human fibroblast senescence and explore the underlying mechanisms. **Methods:** We transfected Alu asRNA into senescent human fibroblasts and used cell counting kit-8 (CCK-8), reactive oxygen species (ROS), and senescence-associated beta-galactosidase (SA-β-gal) staining methods to analyze the anti-aging effects of Alu asRNA on the fibroblasts. We also used an RNA-sequencing (RNA-seq) method to investigate the Alu asRNA-specific mechanisms of anti-aging. We examined the effects of KIF15 on the anti-aging role induced by Alu asRNA. We also investigated the mechanisms underlying a KIF15-induced proliferation of senescent human fibroblasts. **Results:** The CCK-8, ROS and SA-β-gal results showed that Alu asRNA could delay fibroblast aging. RNA-seq showed 183 differentially expressed genes (DEGs) in Alu asRNA transfected fibroblasts compared with fibroblasts transfected with the calcium phosphate transfection (CPT) reagent. The KEGG analysis showed that the cell cycle pathway was significantly enriched in the DEGs in fibroblasts transfected with Alu asRNA compared with fibroblasts transfected with the CPT reagent. Notably, Alu asRNA promoted the KIF15 expression and activated the MEK-ERK signaling pathway. **Conclusion:** Our results suggest that Alu asRNA could promote senescent fibroblast proliferation via activation of the KIF15-mediated MEK-ERK signaling pathway.
Key words: senescent fibroblast; cell proliferation; Alu antisense RNA; KIF15 gene expression; MEK-ERK signaling pathway; cell cycle

Cellular senescence is a kind of state of indefinite proliferative arrest combined with phenotypic changes[1]. Hayflick demonstrated that cultured normal human cells could only divide a limited number of passages before senescence occurred[2]. In this phenomenon, the proliferation ability of senescent human fibroblasts was reduced, cloning ability was decreased, minimum growth cell density was increased, and the cell cycle was elongated[3]. Senescent human fibroblasts also had a higher expression of beta-galactosidase (β-gal), higher reactive oxide species (ROS) levels, increased expression of the senescence gene p16INK4a[4], an irreversible cell cycle arrest[5], and shorter length of telomere[6].

Aged cells affect the physiology and pathology of organisms in complex ways. Although senescent cell accumulation would promote organismal aging and dysfunction[7], senescent cells are beneficial in some cases, such as tissue remodeling, wound repair, and grown prevention of oncogenic cells[4, 8]. The most important cellular component in the dermis is fibroblasts that influence tissue repair. Moreover, skin aging is related to a decrease of the number of fibroblasts, as well as with changes in the morphology and a decrease of the secretion and synthetic function of the fibroblasts[9]. Fibroblasts are the most common cell type of the dermis, and aged fibroblasts contribute to the senescence of the skin[10, 11]. As such, delaying the fibroblast senescence would open new perspectives in the field of skin anti-aging.

The human kinesin superfamily protein (KIF) family contains more than 45 KIFs[12]. KIFs promote

Ning JI, E-mail: 20201011@stu.hebmu.edu.cn
#Corresponding authors, Xiu-fang WANG, E-mail: wangxf1966@hebmu.edu.cn; Zhan-jun LV, E-mail: lslab@hebmu.edu.cn
*This work was supported by grants from the National Natural Science Foundation of China (No. 81771499) and the Natural Science Foundation of Hebei Province, China (No. H2018206099 and No. H2021206460).
Electronic supplementary material The online version of this article (https://doi.org/10.1007/s11596-022-2688-z) contains supplementary material, which is available to authorized users.

the transportation of mRNA, protein complexes, and organelles[13]. They are essential for cell mitosis and meiosis[14, 15]. It has also been reported that KIF15 facilitates the transition of the G1/S phase in pancreatic cancer and upregulates the expression of cyclin D1 and cyclin-dependent kinase 2[16].

Short interspersed nuclear elements (SINEs) account for approximately 10% of the mammalian genomes[17, 18]. Alu elements and B1 elements are the most common SINEs in human and mouse genomes, respectively[19]. Furthermore, the Alu RNA expression is increased under oxidative stress[20, 21], viral infection[22, 23], and during the aging process[24, 25]. Our previous studies also indicated that murine SINE B1 antisense RNA (B1 asRNA) delayed mouse senescence by inhibiting the accumulation of the ROS and regulating the expression of senescence-related genes[26]. Importantly, there were established methods for producing genetically engineered SINE RNAs that were of sufficient quality for *in vitro* for cell experiments and *in vivo* for animal experiments[27, 28].

In this paper, we investigated whether human SINE antisense RNA (Alu antisense RNA; Alu asRNA) could delay or reverse human fibroblast senescence and sought to explore the mechanisms by which Alu asRNA could have this effect. This work could lay the ground work or theoretical basis for the prevention and therapy of skin senescence.

1 MATERIALS AND METHODS

1.1 Human Skin Fibroblast Culture and Transfection

Human skin fibroblasts were derived from the skin of a circumcision patient. Prepuce skin fibroblasts were cultured in Dulbecco's modified Eagle medium (DMEM; ThermoFisher Scientific, USA) with 10% fetal calf serum (FCS; ZETA™ Life, USA) under 5% CO_2 at 37°C. After 6 months of continuous culture, the skin fibroblasts showed the following characteristics of the senescent cells: prolonged cell multiplication time, increased cell volume, multiple cell morphologies, and other senescence characteristics. Some senescent fibroblasts obtained from the culture process were preserved in liquid nitrogen for further study. The study was approved by the Medical Ethics Committee of the Fourth Hospital of Hebei Medical University (approval number: [2020] BC0005).

We used calcium phosphate transfection[29] to transfect Alu sense RNA (Alu RNA), Alu asRNA, and yeast tRNA (tRNA) into senescent fibroblasts, respectively. The sequence of the Alu RNA was GG CTGGGCGCGGTGGCTCACGCCTGTAATCCCAG CACTTTGGGAGGCCGAGGTGGGCGGATCACA AGGTCAGGAGATCAAGACCATCCTGGCTAATA CGGTGAAACCCCGTCTCTACTAAAAATGCAA AAAAATTAGCCGGGTGTGGTGGCGGGTGCCT GTAGTCCCAGCTACTCAAGAGGCTGAGGCAG GAGAATGGCGTGAACCTGGGAGGTGGAGCTT GCAGTGAGCCGAGATCGCGCCACTGCACTCC AGCCTGGGCGACACAGCGAGACTCCGTCTCA. The sequence of the Alu asRNA was TGAGACGGA GTCTCGCTGTGTCGCCCAGGCTGGAGTGCAGT GGCGCGATCTCGGCTCACTGCAAGCTCCACCT CCCAGGTTCACGCCATTCTCCTGCCTCAGCCT CTTGAGTAGCTGGGACTACAGGCACCCGCCA CCACACCCGGCTAATTTTTTTGCATTTTTAGTA GAGACGGGGTTTCACCGTATTAGCCAGGATGG TCTTGATCTCCTGACCTTGTGATCCGCCCACCT CGGCCTCCCAAAGTGCTGGGATTACAGGCGTG AGCCACCGCGCCCAGCC. The base number of the yeast tRNA was 76, which was an RNA control.

Briefly, 6.0×10^4 (unless otherwise stated) senescent fibroblasts were plated in each well of 24-well plates, then cultured at 37°C for 24 h. Fourteen microliters of transfection solution [72 μL of 1 mg/mL RNA, 28 μL of 0.5 mol/L calcium chloride, 54 μL 2×HBS (280 mmol/L of NaCl, 50 mmol/L HEPES, 1.5 mmol/L Na_2HPO_4, and pH 7.05], and 856 μL of double distilled water] was added to the fibroblasts in one well of the 24-well plate. The CPT reagent alone was used as a negative control. The transfected fibroblasts were cultured at 37°C with 5% CO_2. Next, we collected the fibroblasts for the cell proliferation viability, ROS level assays, RT-qPCR, RNA-seq, and Western blotting analysis.

Our previous study used RT-qPCR to measure the transfection efficiency. We used RT-qPCR to assay the relative levels of B1 asRNA in cultured mouse embryo tissue cells after transfection using the CPT reagent. Our results showed that the B1 asRNA level reached its peak at 45 min after transfection. The efficiency of the cellular uptake of the B1 asRNA was approximately 400 molecules per cell at 45 min after transfection[26]. Thus, the SINE antisense RNAs (including Alu asRNA and B1 asRNA) could be efficiently transfected into cultured cells using the CPT reagent.

KIF15 silencing in the fibroblasts was achieved by transfecting the KIF15 siRNA (RiboBio, China) into senescent fibroblasts transfected with Alu asRNA. To transiently transfect the fibroblasts with KIF15 siRNA, ribo*FECT*™ CP reagent was used. KIF15-specific siRNA oligonucleotides were synthesized according to the following target sequences: siKIF15#1, 5′-GGATTCCTATGACAACTTA-3′ and siKIF15#2, 5′-AAACGAATCAGGAGAAAGA-3′. Non-silencing siRNA (siNC, RiboBio, China) was used as a negative control.

1.2 Cell Counting Kit-8 (CCK-8) Assay

CCK-8 (Boster Biological Technology, China) assays were used to assess the fibroblast proliferation viability. Briefly, fibroblasts were seeded in 24-well plates at a density of 6×10^4 cells per well and then cultured at 37°C for 24 h. The fibroblasts were then

transfected with different RNAs for the indicated time. The fibroblasts were changed with 10% fresh FCS-DMEM. Subsequently, 40 μL CCK-8 detection reagents were added into each well and incubated for 1 h at 37°C. A spectrophotometer (Unic UV-2800, China) was used to measure the absorbance (*A*) value at 450 nm.

1.3 ROS Staining

The cytosolic ROS levels in the fibroblasts were determined with a reactive species assay kit (Beyotime Biotechnology, China) that used the cell-permeant indicator molecule 2′, 7′-dichlorodihydrofluorescein diacetate (H_2-DCFH-AD) according to the manufacturer's instructions. The fibroblasts were incubated for 30 min at 20°C with H_2-DCFH-AD, then phosphate-buffered saline (PBS) was used to wash the fibroblasts for three times. The fibroblasts were observed using fluorescent microscopic imaging (Leica, Germany) with a violet blue filter (490 nm). One hundred cells were randomly selected from each sample; Gel-Pro analyzer software (Media Cybernetics, L.P., USA) was used to analyze the integrated optical density (IOD) value of the 100 cells. The total IOD values of the 100 cells represented the fluorescence intensity of this sample. The fluorescence intensity of the CPT reagent group was set as 100%.

1.4 MTT Assay

An MTT assay was used to estimate the cell viability. Briefly, 40 μL MTT (5 mg/mL in PBS) (Fluka, Germany) was added into each well in a 24-well plate. After incubation for 4 h at 37°C, we removed the medium and added 600 μL dimethyl sulfoxide (Tianjin Yongda Chemical Reagent Company Limited, China). A spectrophotometer (Unic UV-2800, China) was used to measure the *A* value at 570 nm.

1.5 Analysis of the T-SOD, GSH-Px Activity, and MDA Levels

The total-superoxide dismutase (T-SOD), glutathione peroxidase (GSH-Px), and malondialdehyde (MDA) kits (Nanjing Jiancheng Bioengineering Institute, China) were used to detect the activity of the T-SOD, GSH-Px, and levels of MDA in the fibroblasts.

1.6 SA-β-gal Cytochemical Assay

A senescence-associated beta-galactosidase (SA-β-gal) staining kit (Beijing Solarbio Science and Technology Co. Ltd., China) was used to determine the SA-β-gal positive percentages of the fibroblasts. The fibroblasts grown in 24-well plates were fixed for 15 min at room temperature using the fixative from the kit. Then, PBS was used to wash the fibroblasts twice for 3 min, SA-β-gal staining solution was added, and the reaction was incubated at 37°C overnight. PBS was used to wash the fibroblasts twice, and the SA-β-gal positive fibroblasts (stained blue-green) were observed under an inverted microscope (Leica, Germany).

1.7 RT-qPCR Analysis of mRNA Expression

To analyze the mRNA expression, TRIzol (Thermo Fisher Scientific, USA) was used to extract the total RNA from the fibroblasts, and DNase I (RNase free; Thermo Fisher Scientific, USA) was used to digest the residual DNA in the presence of RNasin (Thermo Fisher Scientific, USA). 0.5% SDS/5% phenol was used to inactivate the DNase I, and ethyl alcohol was used to precipitate the total RNA. RT-qPCR was performed according to our previous studies[26]. Table 1 shows the primers for RT-qPCR.

1.8 RNA Sequencing (RNA-seq) Analysis

The total RNA was extracted using the TRIzol reagent (Thermo Fisher Scientific, USA). The RNA purity and quantification were evaluated using the NanoDrop 2000 spectrophotometer (Thermo Scientific, USA), and the RNA integrity was assessed using the Agilent 2100 Bioanalyzer (Agilent Technologies, USA). Then, the libraries were constructed using a TruSeq Stranded mRNA LT Sample Prep Kit (Illumina, USA). The RNA-seq analysis was conducted by OE Biotech Co., Ltd. (China) according to the reported references[30–40].

1.9 Western Blotting Analysis

The fibroblasts were lysed with RIPA buffer (Cell Signaling Technology, Inc., USA) and stored at –80°C until the analysis. The protein levels were quantified using the BCA protein assay kit (Solarbio Life Sciences, China). The protein samples (80 μg per lane) were denatured, subjected to 12.5% SDS-PAGE electrophoresis, and transferred onto a nitrocellulose membrane (Pall Corporation, USA). The membrane was blocked and incubated overnight with anti-cyclin E2, anti-CDK1, anti-KIF15, anti-SFN, anti-p-MEK, anti-MEK, anti-p-ERK1/2, or anti-ERK1/2 IgG (Santa Cruz Biotechnology, USA). Anti-β-actin IgG (Santa Cruz Biotechnology, USA) was used as a loading control. After incubation with a horseradish peroxidase-conjugated anti-IgG antibody (Santa Cruz Biotechnology, USA), the blots were developed using the ECL kit (Wanleibio, China) and detected by a chemiluminescence imaging system (Bio-rad, USA). The intensity of each band was normalized to that of β-actin. Gel-Pro analyzer software (Media Cybernetics, L.P., USA) was used to analyze the IOD value of each lane.

1.10 Statistical Analysis

SPSS17.0 software was used for the statistical processing of all data. The differences between the groups were analyzed by one-way ANOVA. The results were expressed as mean±SD, and the values were considered statistically significant at a level of $P<0.05$.

2 RESULTS

2.1 Effects of Alu asRNA on Age-related Changes in Fibroblasts

To determine the effects of Alu asRNA on fibroblast aging, we used cultured senescent fibroblasts

Table 1 Primers used for RT-qPCR in this study

Target	Sequences	Length of the products (bp)
Cyclin E2	Forward: 5′-GCATTATGACACCACCGAAGA-3′	157
	Reverse: 5′-CTAGGGCAATCAATCACAGC -3′	
CDC6	Forward: 5′-CAGTTCAATTCTGTGCCCGC-3′	244
	Reverse: 5′-GCTCCTTCTTGGCTCAAGGT-3′	
CDK1	Forward: 5′-TTTTCAGAGCTTTGGGCACT-3′	195
	Reverse: 5′-CCATTTTGCCAGAAATTCAT-3′	
DLGAP5	Forward: 5′-GTTGTGCAGCCTGTAATGCC-3′	121
	Reverse: 5′-TAGCAGCTCTTGTGACTGGC-3′	
FBXO5	Forward: 5′-CGCTGTAATTCACCTGCAAA-3′	138
	Reverse: 5′-GAGGAGCTTGCCATCTGAAC-3′	
KIF15	Forward: 5′-AGGAATCTGTATTCGCAACTGTG-3′	173
	Reverse: 5′-ACTTCGTGGGATTACTCCTCTC-3′	
PCLAF	Forward: 5′-ATGGTGCGGACTAAAGCAGAC-3′	123
	Reverse: 5′-CCTCGATGAAACTGATGTCGAAT-3′	
RRM2	Forward: 5′-TATATCCCATGTTCTGGCTTTC-3′	100
	Reverse: 5′-GCGGGCTTCTGTAATCTG-3′	
WDHD1	Forward: 5′-GCTTCAGGTCGTCCTAGACAG-3′	159
	Reverse: 5′-CCTTTGGGATGTTACAAGTGGT-3′	
SFN	Forward: 5′-TCCACTACGAGATCGCCAACAG-3′	150
	Reverse: 5′-GTGTCAGGTTGTCTCGCAGCA-3′	
p16INK4a	Forward: 5′-CAGGTCATGATGATGGGCAG-3′	223
	Reverse: 5′-GATGGCCCAGCTCCTCAG-3′	
β-actin	Forward: 5′-TTAATAGTCATTCCAAATATGA-3′	246
	Reverse: 5′-GGGACAAAAAAGGGGGAAGG-3′	

that were continuously cultured for more than 6 months. The senescent fibroblasts were transfected with different RNAs, including Alu RNA, Alu asRNA, tRNA, and CPT reagent. Fig. 1A shows that Alu asRNA transfection induced the fibroblasts to be restored to the state of young fibroblasts: small cell volume, high cell density, and strong three-dimensional sense. However, the fibroblasts in the control groups of the CPT reagent, tRNA, and Alu RNA showed a weak proliferation ability, large cell volume, and low cell density. We also found that Alu asRNA promoted the growth of senescent fibroblasts (fig. 1B).

The viability of the fibroblasts was detected using the CCK-8 assay, which proved that Alu asRNA increased the proliferation viability of the fibroblasts at 48 h and 72 h, respectively after transfection, whereas the Alu RNA and tRNA transfection did not increase the viability of the fibroblasts (fig. 1C). The MTT test results also showed the *A* values of the CPT reagent group, tRNA group, Alu RNA group, and Alu asRNA group were 0.47, 0.42, 0.51, and 0.82, respectively (fig. 1D). These results indicated that Alu asRNA transfection increased the viability of the senescent fibroblasts.

Senescent cells had the characteristic of the high expression of $p16^{INK4a}$. The RT-qPCR results showed that the fibroblasts transfected with Alu asRNA had a significantly reduced $p16^{INK4a}$ gene expression compared with the fibroblasts transfected with the CPT reagent, tRNA, or Alu RNA (fig. 1E).

SA-β-gal is a widely used cytochemical biomarker of aged cells. Fig. 1G shows that the transfection with the CPT reagent, tRNA, Alu RNA, or Alu asRNA induced 83.3%, 81.3%, 78.2%, or 16.0% of the SA-β-gal positive percentages in the fibroblasts. The SA-β-gal positive cell percentage was significantly lower in the cells transfected with Alu asRNA than in cells treated with the CPT reagent, tRNA, or Alu RNA ($P<0.05$; fig.1F and 1G), while the SA-β-gal positive cell percentage in the cells transfected with Alu RNA was not significantly different from that in the cells transfected with the CPT reagent. These results suggested that Alu asRNA significantly decreased the rates of the senescence marker in the senescence fibroblasts. Taken together, our findings showed that Alu asRNA had a positive impact on the senescence fibroblasts.

2.2 Alu asRNA Improves Antioxidant Activities

Specific increases of the ROS level could potentially be critical for the induction and maintenance of the process of cell aging[41]. We, therefore, examined the ROS levels in the fibroblasts using the fluorescent probe H_2-DCFH-AD. Transfection with Alu asRNA resulted in a clearance of the accumulated ROS (fig. 2A). When the fluorescence intensity of the CPT reagent group was set as 100%, the fluorescence intensities of the Alu RNA and Alu asRNA transfection groups were 81.9%, and 21.5%, respectively (fig. 2B). This result illustrated that Alu asRNA cleared the accumulated ROS in the senescent fibroblasts, but Alu RNA did not.

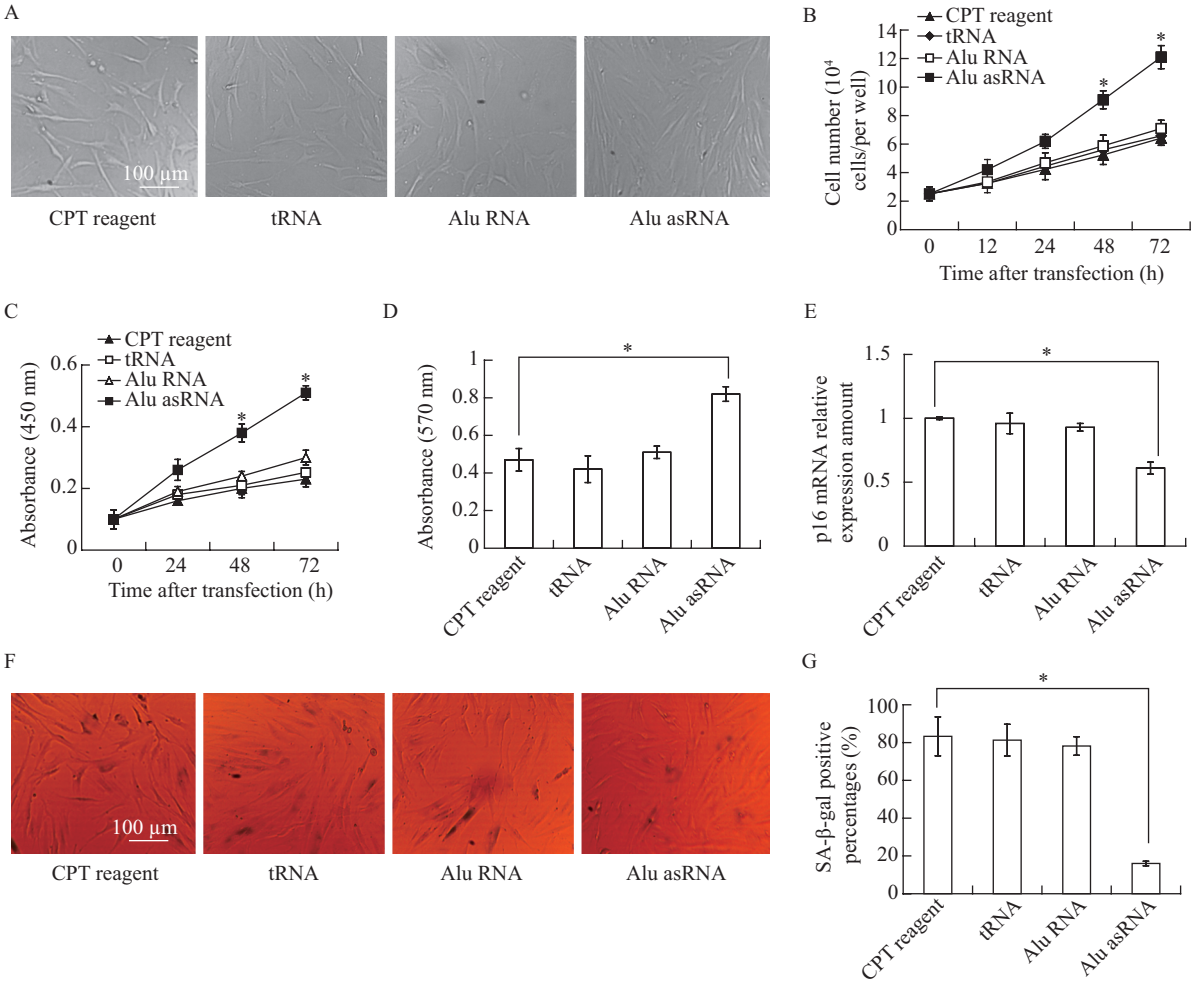

Fig. 1 Effects of Alu asRNA on the age-related changes in the fibroblasts

A: representative cellular morphologies of the CPT reagent group, tRNA group, Alu RNA group, and Alu asRNA group at 72 h after transfection. 2.0×10^4 senescent fibroblasts were plated in each well of a 24-well plate, cultured at a temperature of 37°C for 24 h, then transfected with different RNA, and photographed at 72 h after transfection. B: growth curve of the fibroblasts. The fibroblast growth curve was created by counting the cells at indicated time points. n=3. * indicates that the cell number in the Alu asRNA transfection group was significantly higher than that in the groups of the CPT reagent, tRNA, and Alu RNA. C: detection of cell viability by CCK-8 in the fibroblasts transfected with the CPT reagent alone, tRNA, Alu RNA, or Alu asRNA at different time points. The proliferation activity of the fibroblasts transfected with Alu asRNA was significantly higher than that of the fibroblasts transfected with tRNA, Alu RNA, or CPT reagent alone. The absorbance values at 450 nm are shown as mean±SD of the three independent experiments. D: the MTT detection of the effects of Alu asRNA on promoting the proliferation of the fibroblasts. The results showed that the Alu asRNA transfection promoted cell viability. The absorbance values at 570 nm are shown as mean±SD of the three independent experiments. * indicates that cell viability of the Alu asRNA group was significantly higher than that of the CPT reagent group. E: Alu asRNA decreased the mRNA expression level of $p16^{INK4a}$ in the fibroblasts. * indicates that the $p16^{INK4a}$ mRNA levels were significantly lower in the fibroblasts transfected with Alu asRNA than in the fibroblasts transfected with the CPT reagent (P<0.05). F: representative SA-β-gal staining of the fibroblasts transfected with the CPT reagent, tRNA, Alu RNA, or Alu asRNA. 6.0×10^4 senescent fibroblasts were plated in each well of a 24-well plate, cultured at 37°C for 24 h, and then transfected with different RNAs. SA-β-gal was measured at 72 h after transfection. G: SA-β-gal positive percentages in the fibroblasts (the mean of the three independent experiments). * indicates that the SA-β-gal positive percentage in the Alu asRNA group was lower than that in the CPT reagent group (P<0.05).

Next, we determined the MDA levels in the fibroblasts, which reflected the degree of lipid peroxidation and indirectly reflected the degree of cell damage due to the ROS. Fig. 2C shows that Alu asRNA decreased the MDA levels in the senescent fibroblasts. The MDA level induced by Alu RNA was similar to that induced by the CPT reagent (P=0.662).

We next analyzed the levels of T-SOD, the key enzyme in removing the ROS from the cells by digesting the ROS. Fig. 2D shows that Alu asRNA increased the T-SOD activity in the fibroblasts, but Alu RNA did not.

Senescence cells possess decreased GSH-px activity. Hence, we used the GSH-px kit to determine the GSH-px activity in the fibroblasts. We found that Alu asRNA increased the GSH-px activity in the senescent fibroblasts (P<0.05) (fig. 2E). Alu RNA did not result in a significant difference in the GSH-px

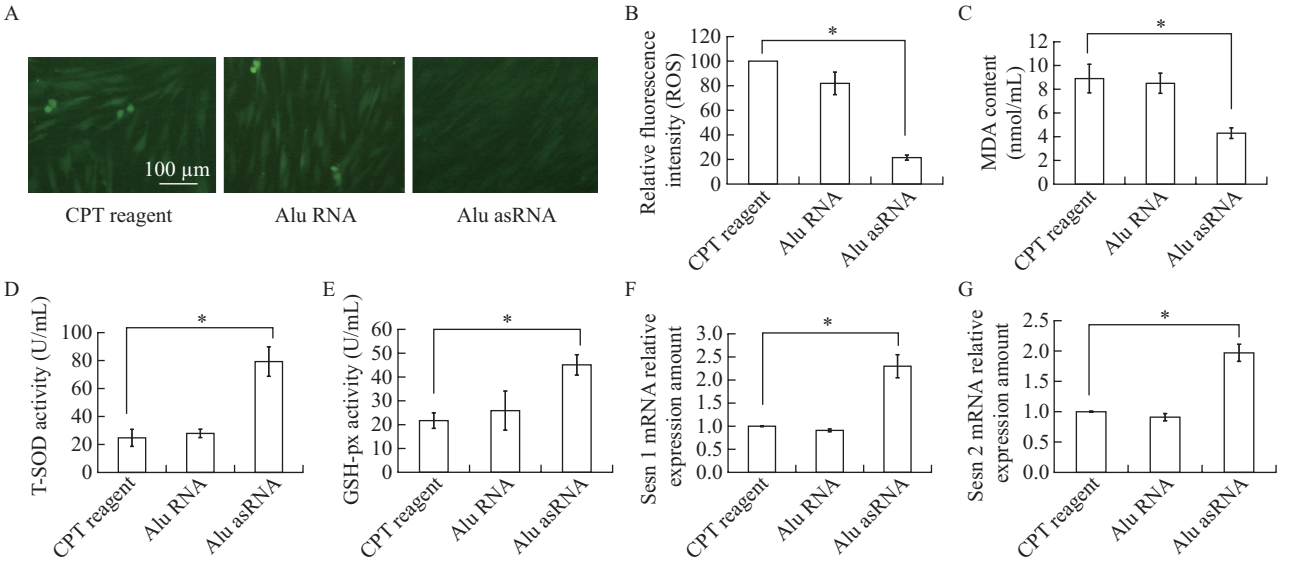

Fig. 2 Alu asRNA increases the antioxidant protection in the senescence fibroblasts

A: representative images of the ROS levels in the fibroblasts transfected with the CPT reagent, Alu RNA, or Alu asRNA. B: relative fluorescence intensity of the images shown in fig. 2A. The CPT reagent transfection group was set as 100%. The fluorescence levels were corrected to account for the image's background. n=3. $^*P$<0.05. C: Alu asRNA decreased the MDA content. $^*P$<0.05. D: Alu asRNA increased the activity of T-SOD. $^*P$<0.05. E: Alu asRNA increased the activity of GSH-px. $^*P$<0.05. F: Alu asRNA increased the mRNA levels of the Sesn 1 gene. $^*P$<0.05. G: Alu asRNA increased the mRNA levels of the Sesn 2 gene. $^*P$<0.05

activity compared to transfection with the CPT reagent (P=0.456).

As the sestrins Sesn 1 and Sesn 2 were important anti-oxidant proteins[42], we assessed the Sesn 1 and Sesn 2 mRNA levels by RT-qPCR. fig. 2F and G show that Alu asRNA increased the mRNA levels of the Sesn 1 and Sesn 2 genes, but Alu RNA did not.

2.3 RNA-seq Analysis of the Alu asRNA-Transfected Fibroblasts

To investigate the molecular mechanisms of Alu asRNA underlying anti-aging, we analyzed the gene expression profile of the Alu asRNA-transfected fibroblasts using RNA-seq. Although some characters were controlled by a single gene, such as monogenic disorders, cellular aging involved changes in the gene expression regulation that would usually involve more than one gene. If multiple genes underwent small changes simultaneously (fold-change ≥1.5 or ≤0.67), the accumulation of these changes would lead to significant impacts on the characters. Thus, we determined the number of genes that were upregulated or downregulated (fold-change≥1.5 or ≤0.67; P<0.05) and adjusted for multiple comparisons in the fibroblasts transfected with the CPT reagent alone with Alu RNA, or with Alu asRNA. We found 149 differentially expressed genes (DEGs) among which 71 were upregulated genes and 78 were downregulated genes in the fibroblasts transfected with Alu RNA compared with the fibroblasts transfected with the CPT reagent (table S1; fig. 3A). We also identified 183 DEGs, including 96 upregulated genes and 87 downregulated genes, in the Alu asRNA transfected fibroblasts compared with the fibroblasts transfected with the CPT reagent (table S2; fig. 3A). In fig. 3B, a volcano plot shows the overall distribution of the DEGs in the fibroblasts transfected with Alu RNA compared with the fibroblasts transfected with the CPT reagent; fig. 3C shows the overall distribution of the DEGs in the fibroblasts transfected with Alu asRNA compared with the fibroblasts transfected with the CPT reagent.

To explore the potential biological functions of the DEGs, we performed gene ontology (GO) enrichment analyses, including the molecular functions (MF), cellular components (CC), and biological processes (BP). For the comparison of the Alu RNA transfection with the cells transfected with the CPT reagent, changes in the BP of the DEGs were significantly enriched in the DNA replication checkpoint, positive regulation of the kinase activity, hemidesmosome assembly, etc. (fig. 3D). For the CC, the DEGs were mainly enriched in the intermediate filament, cortical actin cytoskeleton, mitotic spindle, etc. Within the MF category, the DEGs were mainly enriched in epinephrine binding, transmembrane receptor protein tyrosine kinase activity, structural constituent of cytoskeleton, etc. (fig. 3D).

In the GO enrichment results for the comparison of the Alu asRNA transfection with the cells transfected with the CPT reagent, for the BP, the DEGs were mainly enriched in the DNA replication, DNA-dependent DNA replication, mitotic cell cycle, etc. (fig. 3E). For the CC, the DEGs were mainly enriched in the spindle, extracellular matrix, collagen-containing extracellular matrix, etc. For the MF, the

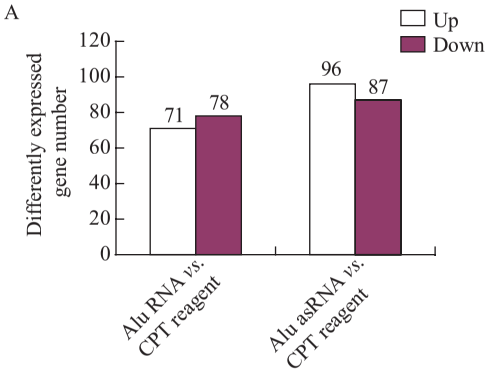
A
Up
Down
Differently expressed gene number
120
100
80
60
40
20
0
71
78
96
87
Alu RNA vs. CPT reagent
Alu asRNA vs. CPT reagent

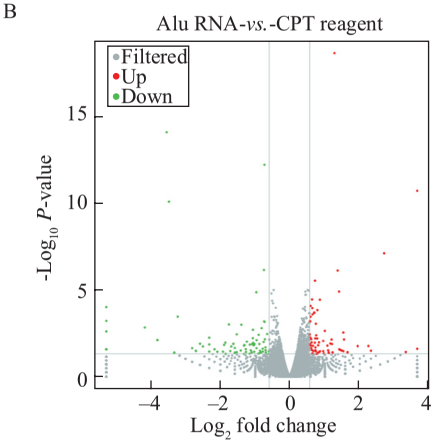
B
Alu RNA-vs.-CPT reagent
Filtered
Up
Down
-Log10 P-value
15
10
5
0
−4
−2
0
2
4
Log2 fold change

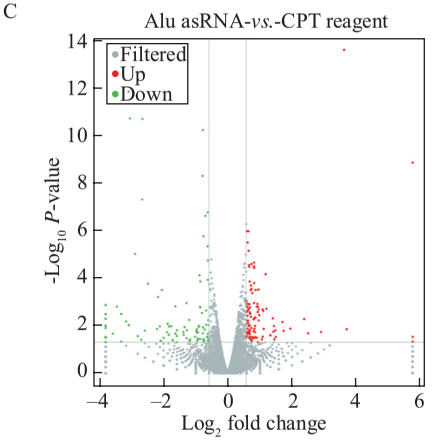
C
Alu asRNA-vs.-CPT reagent
Filtered
Up
Down
-Log10 P-value
14
12
10
8
6
4
2
0
−4
−2
0
2
4
6
Log2 fold change

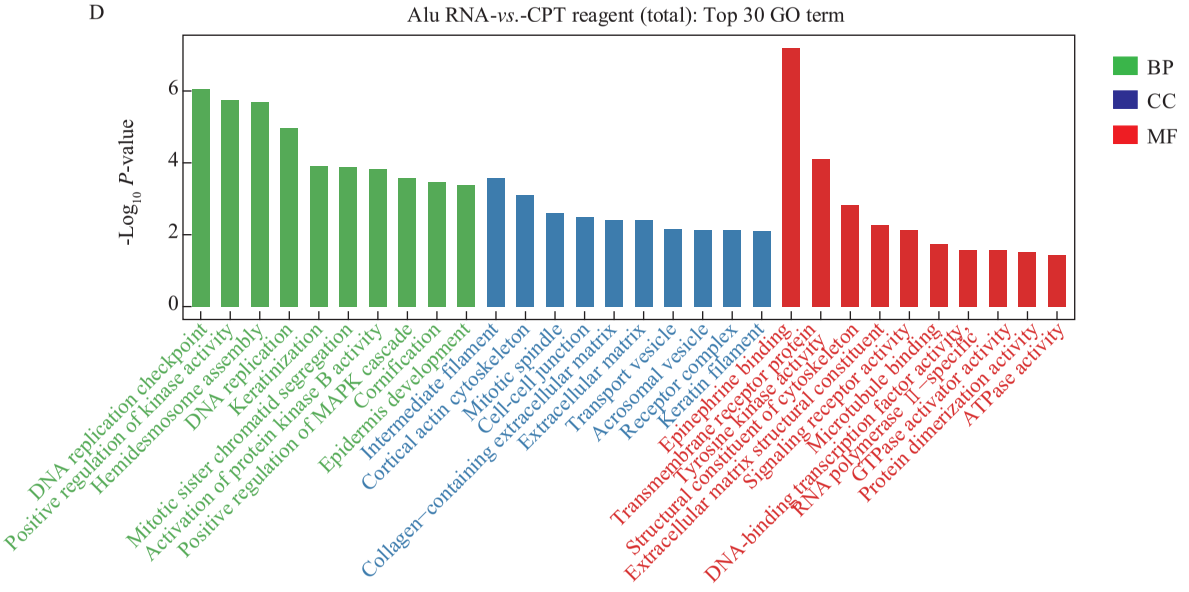
D
Alu RNA-vs.-CPT reagent (total): Top 30 GO term
-Log10 P-value
6
4
2
0
BP
CC
MF
DNA replication checkpoint
Positive regulation of kinase activity
Hemidesmosome assembly
DNA replication
Keratinization
Mitotic sister chromatid segregation
Activation of protein kinase B activity
Positive regulation of MAPK cascade
Cornification
Epidermis development
Intermediate filament
Cortical actin cytoskeleton
Mitotic spindle
Cell-cell junction
Collagen−containing extracellular matrix
Extracellular matrix
Transport vesicle
Acrosomal vesicle
Receptor complex
Keratin filament
Epinephrine receptor protein
Transmembrane receptor protein
Tyrosine kinase activity
Structural constituent of cytoskeleton
Extracellular matrix structural constituent
Signaling receptor activity
Microtubule binding
DNA-binding transcription factor activity
RNA polymerase II−specific
GTPase activator activity
Protein dimerization activity
ATPase activity

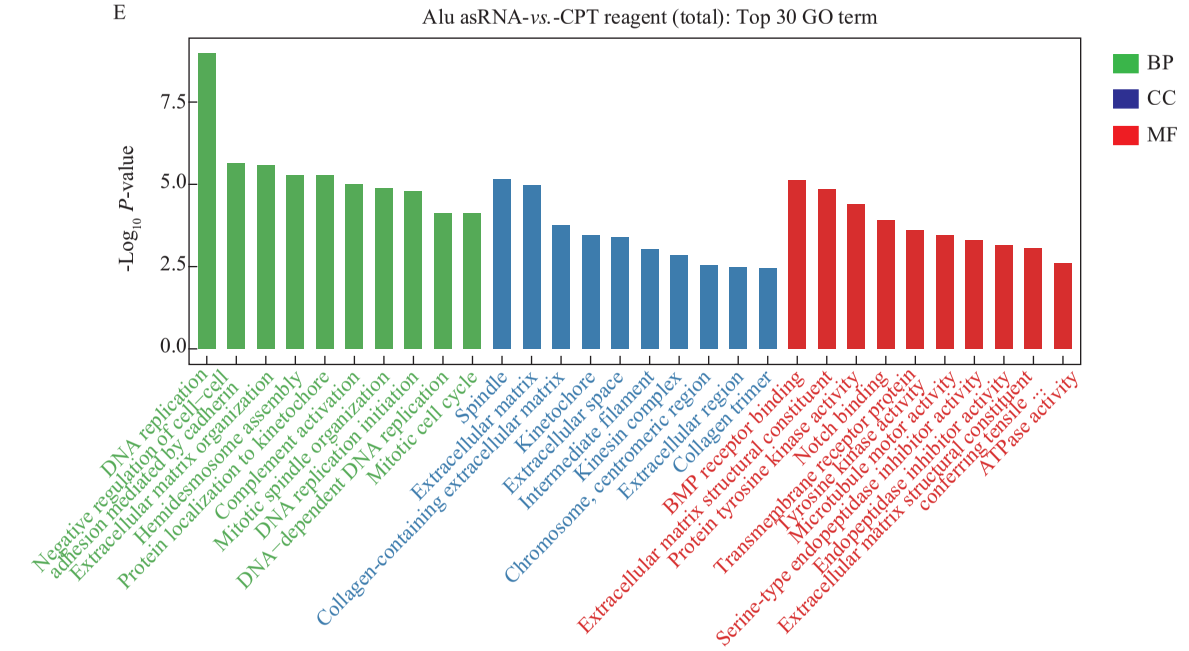
E
Alu asRNA-vs.-CPT reagent (total): Top 30 GO term
-Log10 P-value
7.5
5.0
2.5
0.0
BP
CC
MF
DNA replication
Negative regulation of cell−cell adhesion mediated by cadherin
Extracellular matrix organization
Hemidesmosome assembly
Protein localization to kinetochore
Complement activation
Mitotic spindle organization
DNA replication initiation
DNA−dependent DNA replication
Mitotic cell cycle
Collagen-containing extracellular matrix
Spindle
Extracellular matrix
Kinetochore
Extracellular space
Intermediate filament
Kinesin complex
Chromosome, centromeric region
Extracellular region
Collagen trimer
BMP receptor binding
Extracellular matrix structural constituent
Protein tyrosine kinase activity
Transmembrane receptor protein
Tyrosine kinase activity
Microtubule motor activity
Endopeptidase inhibitor activity
Serine-type endopeptidase inhibitor activity
Extracellular matrix structural constituent conferring tensile ...
ATPase activity

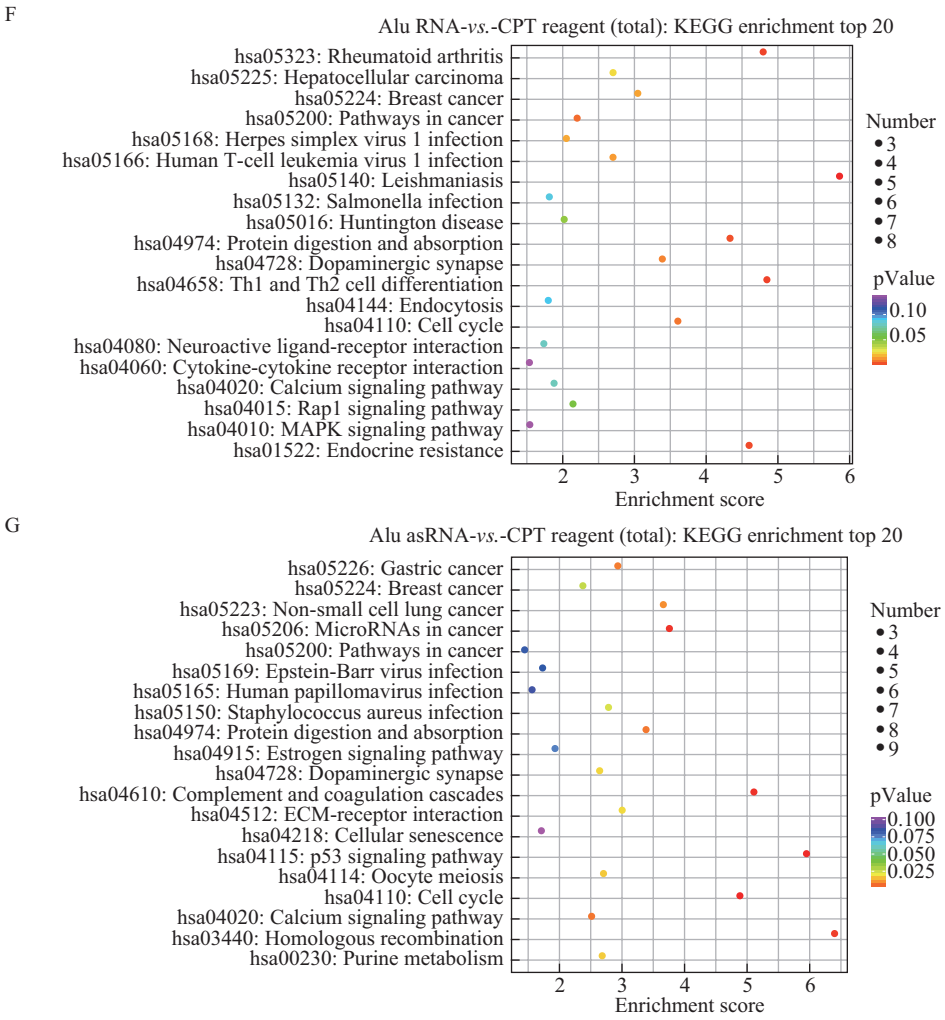

Fig. 3 Identification and enrichment analyses of differentially expressed genes (DEGs)

A: histogram of the DGEs. B: the overall distribution of the DEGs in the fibroblasts transfected with Alu RNA compared with the fibroblasts transfected with the CPT reagent. The gray dots represent the genes without significant differences, the green dots represent the downregulated DEGs, and the red dots represent the upregulated DEGs. C: the overall distribution of the DEGs in the fibroblasts transfected with Alu asRNA compared with the fibroblasts transfected with the CPT reagent. The gray dots represent the genes without significant differences. The green dots represent the downregulated DEGs, and the red dots represent the upregulated DEGs. D: enriched GO terms of the DEGs in the fibroblasts transfected with Alu RNA compared with the fibroblasts transfected with the CPT reagent. E: enriched GO terms of the DEGs in the fibroblasts transfected with Alu asRNA compared with the fibroblasts transfected with the CPT reagent. F: the KEGG pathways of the DEGs in the fibroblasts transfected with Alu RNA compared with the fibroblasts transfected with the CPT reagent. G: The KEGG pathways of the DEGs in the fibroblasts transfected with Alu asRNA compared with the fibroblasts transfected with the CPT reagent.

DEGs were mainly enriched in the BMP receptor binding, extracellular matrix structural constituent, protein tyrosine kinase activity, etc. These findings suggested that the GO function of the DEGs induced by the Alu asRNA transfection was associated with the DNA replication initiation, DNA-dependent DNA replication, and mitotic cell cycle.

When we performed a Kyoto Encyclopedia of Genes and Genomes (KEGG) enrichment analysis, pathways in cancer, herpes simplex virus 1 infection, and neuroactive ligand-receptor interaction were significantly enriched in the DEGs in the fibroblasts transfected with Alu RNA compared with those in the fibroblasts transfected with the CPT reagent (fig. 3F). MicroRNAs in cancer, complement and coagulation cascades, p53 signaling pathway, cell cycle, etc. were significantly enriched in the DEGs in the fibroblasts transfected with Alu asRNA compared with the fibroblasts transfected with the CPT reagent (fig. 3G). These findings suggested that the cell cycle was significantly enriched in the DEGs in the fibroblasts transfected with Alu asRNA compared to the fibroblasts transfected with the CPT reagent.

2.4 Effects of Alu asRNA on the Expression of the Cell Cycle Genes

Fig. 3G shows that the cell cycle was significantly enriched in the DEGs in the fibroblasts transfected with Alu asRNA compared to the fibroblasts transfected with the CPT reagent. Then, we analyzed the DEGs that affected the cell cycle. The RNA-seq results

Table 2 Sensitivity and specificity for the ROC curve analysis

Gene_id	Fold change	*P*-value	Regulation	Description
BARD1	2.271269662	7.09E-05	Up	BRCA1 associated RING domain 1
Cyclin E2	1.885611856	0.001635	Up	Cyclin E2
CDC6	1.66431425	0.000209	Up	Cell division cycle 6
CDK1	1.678466964	2.63E-05	Up	Cyclin dependent kinase 1
CENPF	1.591031942	2.96E-05	Up	Centromere protein F
CHAF1B	1.513429877	0.01897	Up	Chromatin assembly factor 1 subunit B
DLGAP5	1.648929146	0.000331	Up	DLG associated protein 5
E2F5	1.655741106	0.038098	Up	E2F transcription factor 5
FBXO5	1.535061223	0.003944	Up	F-box protein 5
HASPIN	2.653317743	0.005014	Up	Histone H3 associated protein kinase
HMMR	1.546466944	0.006594	Up	Hyaluronan mediated motility receptor
KIF15	1.67738478	0.01275	Up	Kinesin family member 15
MCM10	1.821767268	0.0047	Up	Minichromosome maintenance 10 replication initiation factor
ORC6	1.576108718	0.018549	Up	Origin recognition complex subunit 6
PBK	1.531699568	0.001648	Up	PDZ binding kinase
PCLAF	1.610289389	0.001283	Up	PCNA clamp associated factor
RGCC	1.561703071	0.008244	Up	Regulator of cell cycle
RRM2	1.574835574	1.12E-06	Up	Ribonucleotide reductase regulatory subunit M2
SFN	0.335476956	0.015742	Down	Stratifin
TIPIN	1.979314041	0.003669	Up	TIMELESS interacting protein
TTK	1.773628169	0.001142	Up	TTK protein kinase
WDHD1	1.626673147	0.001744	Up	WD repeat and HMG-box DNA binding protein 1
XRCC2	1.957965507	0.006131	Up	X-ray repair cross complementing 2

showed that there were 22 upregulated cell cycle DEGs and one downregulated cell cycle DEG (table 2). We chose nine upregulated and one downregulated (i.e., SFN gene) cell cycle DEGs for detecting the mRNA expression through RT-qPCR. The selected nine upregulated genes consisted of Cyclin E2, CDC6, CDK1, DLGAP5, FBXO5, KIF15, PCLAF, RRM2, and WDHD1. The reason why we selected these nine genes for the RT-qPCR validation was that they had relatively high expression abundance.

We found that the results of the RT-qPCR were consistent with those of the RNA-seq (fig. 4A). Next, we used Western blotting analysis to detect the effects of Alu asRNA on the protein expression of Cyclin E2, CDK1, KIF15, and SFN. Fig. 4B shows that Alu asRNA increased the protein expression levels of Cyclin E2, CDK1, KIF15 and decreased the protein expression of SFN.

2.5 KIF15 Plays a Critical Role in Reversing Fibroblast Senescence

KIF15 is believed to promote G1/S phase transition and is a critical gene that promotes cell proliferation[16]. To determine the roles of KIF15 in promoting senescent fibroblast proliferation, senescent fibroblasts were transfected with Alu asRNA and then transfected with either the control or KIF15 siRNA. Western blotting analysis suggested that siRNA-KIF15 could significantly inhibit the expression of KIF15 at the protein level (fig. 5A and 5B).

To detect the proliferative ability of the fibroblasts, we used the CCK-8 assay. Our results showed that the proliferation viability of the fibroblasts decreased significantly when the fibroblasts were treated with KIF15 siRNA ($P<0.05$; fig. 5C). The KIF15 siRNA treatment eliminated the lowering effects of Alu asRNA on the positive percentage of SA-β-gal (fig. 5D). The proportion of positive cells was significantly higher in the fibroblasts treated with Alu asRNA + KIF15 siRNA than in fibroblasts treated with Alu asRNA (fig. 5E; $P<0.05$). These results demonstrated that KIF15 played a critical role in reversing fibroblast senescence.

2.6 Alu asRNA Activated the MEK-ERK Pathway

As the MEK-ERK signaling pathway was closely connected with KIF15[16], we investigated whether the expression changes of the KIF15 gene could affect the activation of the MEK-ERK signaling pathway. Fig. 6A shows that the Alu asRNA transfection increased the protein expression of KIF15, p-ERK, and p-ERK1/2. In addition, the KIF15 knockdown inhibited the protein expression of KIF15, p-ERK, and p-ERK1/2 (fig. 6A). To investigate whether the MEK-ERK pathway mediated the effect, the fibroblasts transfected with Alu asRNA were treated with PD98059, a kind of MEK-ERK pathway inhibitor. The CCK-8 assays showed that the enhancement of cell viability induced by Alu asRNA was counteracted by treatment with PD98059 (fig. 6B), thus indicating that the effects of Alu asRNA on senescent fibroblasts were mediated by the MEK-ERK signaling pathway.

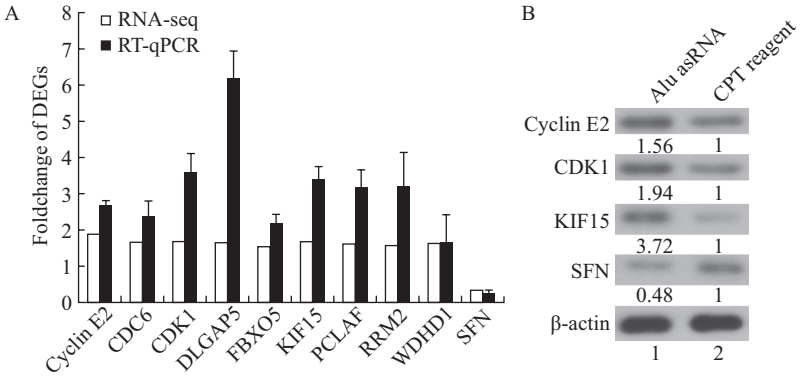

Fig. 4 Alu asRNA transfection affected the expression of cell cycle genes

A: comparison of the RT-qPCR detection results with the RNA-seq results. The Y-axis represents the fold change of the gene expression for the Alu asRNA transfection group compared with that of the CPT reagent treatment. The RT-qPCR detection showed that the Alu asRNA transfection increased the mRNA levels of the cell cycle genes, including those of Cyclin E2, CDC6, CDK1, DLGAP5, FBXO5, KIF15, PCLAF, RRM2, and WDHD1. In contrast, Alu asRNA decreased the SFN mRNA level. B: The protein expression levels of Cyclin E2, CDK1, KIF15, and SFN were analyzed by Western blotting analysis in the fibroblasts transfected with Alu asRNA compared with the fibroblasts transfected with the CPT reagent. n=3. The numbers "1 and 2" under the β-actin bands represent the number of lanes.

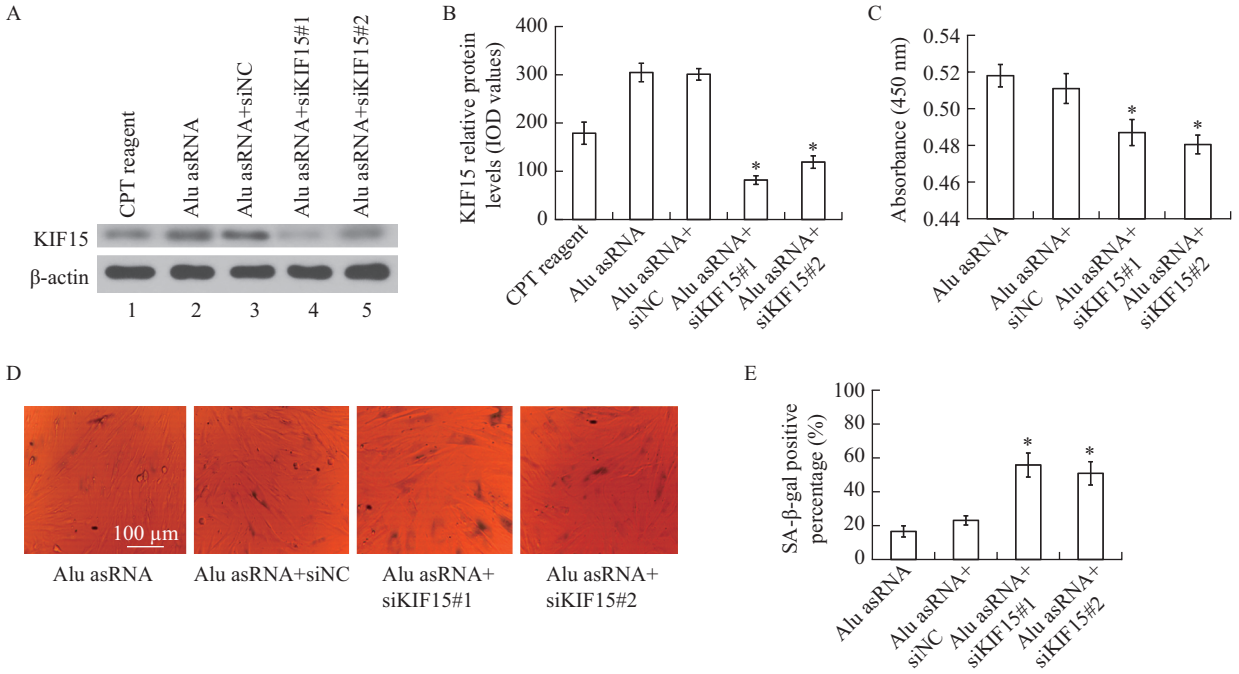

Fig. 5 KIF15 promotes the proliferation activity and reverses the senescence of the fibroblasts

A: The effect of the KIF15 knockdown with siRNA was verified by the Western blotting analysis. B: The amount of protein (IOD value) per lane for fig. 5A. n=3. The asterisk indicates that the protein expression of KIF15 was significantly lower in the fibroblasts treated with Alu asRNA+KIF15 siRNA than in the fibroblasts treated with Alu asRNA. C: The cell proliferation activity significantly decreased when the fibroblasts were treated with KIF15 siRNA. $^*P$<0.05. D: Representative SA-β-gal staining of the fibroblasts treated with Alu asRNA, Alu asRNA+siNC, Alu asRNA+siKIF15#1, and Alu asRNA+siKIF15#2. E: quantification of the SA-β-gal positive percentages (SA-β-gal positive cell number/total cell number ×100%) in fig. 5D (the mean of the three independent experiments). The asterisk indicates that the positive cell percentage in the Alu asRNA+siKIF15#1 or Alu asRNA+siKIF15#2 group was significantly higher than that of the Alu asRNA group (P<0.05).

3 DISCUSSION

Senescent morphology and permanent loss of proliferative potential are the important characteristics of aged cells[43]. In the present study, Alu asRNA improved the cellular aging phenotype and reduced the ROS levels, $p16^{INK4a}$ gene expression, and SA-β-gal positive percentages. These results suggested that Alu asRNA possessed anti-aging effects on senescent fibroblasts.

The Alu RNA level increase could result in proliferation suppression, viability decrease, and apoptotic induction in human cells[44, 45]. Furthermore, Alu RNA analogs suppressed the MCF-7 cell viability via regulating expression of the regulator NUPR1 (p8) and the transcription factor DDIT3[45].

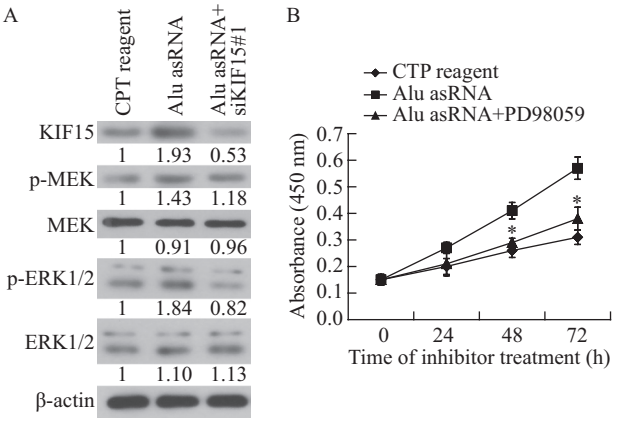

Fig. 6 Alu asRNA activated the MEK-ERK signaling pathway
A: Western blot analysis was used to detect the protein expression levels of the key modulators of the MEK-ERK signaling pathway in the fibroblasts treated with the CPT reagent, Alu asRNA, or Alu asRNA+siKIF15#1. n=3. The fibroblasts were transfected with the CPT reagent, or Alu asRNA, and after 48 h, the fibroblasts transfected with Alu asRNA were transfected with siKIF15#1. The protein expression levels were detected using Western blotting analysis at 48 h after the siKIF15#1 transfection. B: The MEK-ERK signaling pathway inhibitor PD98059 inhibited the cell viability. The fibroblasts were treated with the CPT reagent, Alu asRNA, or Alu asRNA+PD98059 (25 μmol/L), and the CCK-8 assay was used to measure the proliferation rates of the fibroblasts at different time points. The proliferation activity of the fibroblasts treated with Alu asRNA+PD98059 was significantly lower than that of the fibroblasts transfected with Alu asRNA ($^*P$<0.05). The absorbance values at 450 nm were the mean±SD of the three independent experiments.

Moreover, the Alu RNA accumulation activated NLRP3 inflammasome and downstream apoptotic proteins related to geographic atrophy, and Alu RNA antisense oligonucleotide proved to be effective for treating geographic atrophy[45]. Alu RNA regulated the expression of several genes *via* binding with proteins of initiating the apoptotic pathway[26, 46]. Therefore, we speculated that Alu asRNA would play its role by binding Alu RNA.

An irreversible cell cycle arrest is regarded as an important mechanism of cell aging[47]. As such, the RNA-seq results revealed that Alu asRNA activated the cell cycle of the senescent fibroblasts. Alu asRNA transfection also increased the expression of 23 cell cycle genes, including Cyclin E2, CDK1, KIF15, etc. (table 2).

In addition, KIF15 played an important role in cell division, tumor cell proliferation, and cell cycle regulation[48–54]. KIF15 promotes proliferation of pancreatic cancer cells via the MEK-ERK signaling pathway[16]. The MEK-ERK signaling pathway is involved in controlling the cell proliferation and survival process[55, 56]. The role of KIF15 in anti-aging or reversing of aging has previously been unknown and presented a new characteristic of KIF15. Our study revealed that Alu asRNA promoted the proliferation of senescent fibroblasts by activating the KIF15 expression and identified a potential link between the KIF15 promotion proliferation effects and the MEK-ERK signaling pathway.

In summary, our study provided evidence that the transfection of senescent human fibroblasts with Alu asRNA reversed age-related changes in human fibroblasts. Furthermore, Alu asRNA appeared to promote the cell cycle processes via a KIF15-medicated MEK-ERK signaling pathway. Overall, human Alu asRNA could serve as an effective nucleic acid drug for treatment of human skin aging.

Conflict of Interest Statement

The authors declare no conflicts of interests related to this study.

REFERENCES

1 Rhinn M, Ritschka B, Keyes WM. Cellular senescence in development, regeneration and disease. Development, 2019,146(20):dev151837
2 Shay JW, Wright WE. Hayflick, his limit, and cellular ageing. Nat Rev Mol Cell Biol, 2000,1(1):72-76
3 Hsu WH, Lin BZ, Leu JD, *et al*. Involvement of 8-O-acetylharpagide for Ajuga taiwanensis mediated suppression of senescent phenotypes in human dermal fibroblasts. Sci Rep, 2020,10(1):19731
4 Baker DJ, Childs BG, Durik M, *et al*. Naturally occurring p16(Ink4a)-positive cells shorten healthy lifespan. Nature, 2016,30(7589):184-189
5 Campisi J. Senescent cells, tumor suppression, and organismal aging: good citizens, bad neighbors. Cell, 2005,120(4):513-522
6 Zannas AS, Kosyk O, Leung CS. Prolonged glucocorticoid exposure does not accelerate telomere shortening in cultured human fibroblasts. Genes (Basel), 2020,11(12):1425
7 Di Micco R, Krizhanovsky V, Baker D, *et al*. Cellular senescence in ageing: from mechanisms to therapeutic opportunities. Nat Rev Mol Cell Biol, 2021,22(2):75-95
8 He S, Sharpless NE. Senescence in health and disease. Cell, 2017,169(6):1000-1011
9 Kurban RS, Bhawan J. Histologic changes in skin associated with aging. J Dermatol Surg Oncol, 1990,16(10):908-914
10 Gruber F, Kremslehner C, Eckhart L, *et al*. Cell aging and cellular senescence in skin aging -Recent advances in fibroblast and keratinocyte biology. Exp Gerontol, 2020,130:110780
11 Demaria M, Ohtani N, Youssef SA, *et al*. An essential role for senescent cells in optimal wound healing through secretion of PDGF-AA. Dev Cell, 2014,31(6):722-733
12 Zhou L, Ouyang L, Chen K, *et al*. Research progress on KIF3B and related diseases. Ann Transl Med, 2019,7(18):492
13 Brendza RP, Serbus LR, Duffy JB, *et al*. A function for kinesin I in the posterior transport of oskar mRNA and Staufen protein. Science, 2000,289(5487):2120-2122
14 Vicente JJ, Wordeman L. Mitosis, microtubule

dynamics and the evolution of kinesins. Exp Cell Res, 2015,334(1):61-69
15 Sharp DJ, Rogers GC, Scholey JM. Microtubule motors in mitosis. Nature, 2000,407(6800):41-47
16 Wang J, Guo X, Xie C, *et al*. KIF15 promotes pancreatic cancer proliferation via the MEK-ERK signalling pathway. Br J Cancer, 2017,117(2):245-255
17 Nellåker C, Keane TM, Yalcin B, *et al*. The genomic landscape shaped by selection on transposable elements across 18 mouse strains. Genome Biol, 2012,13(6):R45
18 Walters-Conte KB, Johnson DL, Allard MW, *et al*. Carnivore-specific SINEs (Can-SINEs): distribution, evolution, and genomic impact. J Hered, 2011,102 Suppl 1(Suppl 1):S2-S10
19 Richardson SR, Doucet AJ, Kopera HC, *et al*. The Influence of LINE-1 and SINE Retrotransposons on Mammalian Genomes. Microbiol Spectr, 2015,3(2):MDNA3-0061-2014
20 Hwang YE, Baek YM, Baek A, *et al*. Oxidative stress causes Alu RNA accumulation via PIWIL4 sequestration into stress granules. BMB Rep, 2019,52(3):196-201
21 Wang W, Wang WH, Azadzoi KM, *et al*. Alu RNA accumulation in hyperglycemia augments oxidative stress and impairs eNOS and SOD2 expression in endothelial cells. Mol Cell Endocrinol, 2016,426:91-100
22 Crooke PS 3rd, Tossberg JT, Porter KP, *et al*. Cutting Edge: reduced adenosine-to-inosine editing of endogenous Alu RNAs in severe COVID-19 disease. J Immunol, 2021,206(8):1691-1696
23 Aune TM, Tossberg JT, Heinrich RM, *et al*. Alu RNA structural features modulate immune cell activation and A-to-I editing of Alu RNAs is diminished in human inflammatory bowel disease. Front Immunol, 2022,13:818023
24 Yamada K, Kaneko H, Shimizu H, *et al*. Lamivudine inhibits Alu RNA-induced retinal pigment epithelium degeneration via anti-inflammatory and anti-senescence activities. Transl Vis Sci Technol, 2020,9(8):1
25 Bravo JI, Nozownik S, Danthi PS, *et al*. Transposable elements, circular RNAs and mitochondrial transcription in age-related genomic regulation. Development, 2020,147(11):dev175786
26 Song Z, Shah S, Lv B, *et al*. Anti-aging and anti-oxidant activities of murine short interspersed nuclear element antisense RNA. Eur J Pharmacol, 2021,912:174577
27 Liu C, Zhao Y, Yin S, *et al*. The expression and construction of engineering Escherichia coli producing humanized AluY RNAs. Microb Cell Fact, 2017,16(1):183
28 Khan M, Yan L, Lv B, *et al*. The preparation of endotoxin-free genetically engineered murine B1 antisense RNA. Anal Biochem, 2020,599:113737
29 Kwon M, Firestein BL. DNA transfection: calcium phosphate method. Methods Mol Biol, 2013,1018:107-110
30 Bolger AM, Lohse M, Usadel B. Trimmomatic: a flexible trimmer for Illumina sequence data. Bioinformatics, 2014,30(15):2114-2120
31 Kim D, Langmead B, Salzberg SL. HISAT: a fast spliced aligner with low memory requirements. Nature Methods, 2015,12(4):357-360
32 Das S, Rai SN. Statistical methods for analysis of single-cell RNA-sequencing data. MethodsX, 2021,8:101580
33 Trapnell C, Williams BA, Pertea G, *et al*. Transcript assembly and quantification by RNA-Seq reveals unannotated transcripts and isoform switching during cell differentiation. Nat Biotechnol, 2010,28(5):511-515
34 Anders S, Pyl PT, Huber W. HTSeq--a Python framework to work with high-throughput sequencing data. Bioinformatics, 2015,31(2):166-169
35 Nirgude S, Desai S, Choudhary B. Curcumin alters distinct molecular pathways in breast cancer subtypes revealed by integrated miRNA/mRNA expression analysis. Cancer Rep (Hoboken), 2022,5(10):e1596
36 Wang J, Zhao K, Chen L, *et al*. Proteomics and post-translational modifications analysis of umbilical mesenchymal stem cells aging. Anal Biochem, 2022,652:114770
37 Pertea M, Pertea GM, Antonescu CM, *et al*. StringTie enables improved reconstruction of a transcriptome from RNA-seq reads. Nat Biotechnol, 2015,33(3):290-295
38 Li H, Handsaker B, Wysoker A, *et al*. The sequence alignment/map (SAM) format and SAMtools. Bioinformatics, 2009,25(16):2078-2079
39 Li H. A statistical framework for SNP calling, mutation discovery, association mapping and populationgenetical parameter estimation from sequencing data. Bioinformatics, 2011,27(21):2987-2993
40 Cingolani P, Platts A, Wang le L, *et al*. A program for annotating and predicting the effects of single nucleotide polymorphisms, SnpEff: SNPs in the genome of Drosophila melanogaster strain w1118; iso-2; iso-3. Fly (Austin), 2012,6(2):80-92
41 Qi M, Zhou H, Fan S, *et al*. mTOR inactivation by ROS-JNK-p53 pathway plays an essential role in psedolaric acid B induced autophagy-dependent senescence in murine fibrosarcoma L929 cells. Eur J Pharmacol, 2013,715(1-3):76-88
42 Mao X, Fang W, Liu Q. An emerging role of Alu RNA in geographic atrophy pathogenesis: the implication for novel therapeutic strategies. Discov Med, 2016,22(123):337-349
43 Romanov VS, Abramova MV, Svetlikova SB, *et al*. p21 (Waf1) is required for cellular senescence but not for cell cycle arrest induced by the HDAC inhibitor sodium butyrate. Cell Cycle, 2010,9(19):3945-3955
44 Li M, Larsen PA. Primate-specific retrotransposons and the evolution of circadian networks in the human brain. Neurosci Biobehav Rev, 2021,131:988-1004
45 Baryakin DN, Semenov DV, Savelyeva AV, *et al*. Alu- and 7SL RNA analogues suppress MCF-7 cell viability through modulating the transcription of endoplasmic reticulum stress response genes. Acta Naturae, 2013,5(4):83-93
46 Wang J, Geesman GJ, Hostikka SL, *et al*. Inhibition of activated pericentromeric SINE/Alu repeat transcription in senescent human adult stem cells reinstates self-renewal. Cell Cycle, 2011,10(17):3016-3030
47 van Deursen JM. The role of senescent cells in ageing. Nature, 2014,09(7501):439-446
48 Klejnot M, Falnikar A, Ulaganathan V, *et al*. The crystal structure and biochemical characterization of Kif15: a

bifunctional molecular motor involved in bipolar spindle formation and neuronal development. Acta Crystallogr D Biol Crystallogr, 2014,70(Pt 1):123-133
49 Florian S, Mayer TU. Modulated microtubule dynamics enable Hklp2/Kif15 to assemble bipolar spindles. Cell Cycle, 2011,10(20):3533-3544
50 Messin LJ, Millar JB. Role and regulation of kinesin-8 motors through the cell cycle. Syst Synth Biol, 2014,8(3):205-213
51 Drechsler H, McHugh T, Singleton MR, *et al*. The Kinesin-12 Kif15 is a processive track-switching tetramer. eLife, 2014,3:e01724
52 Buster DW, Baird DH, Yu W, *et al*. Expression of the mitotic kinesin Kif15 in postmitotic neurons: implications for neuronal migration and development. J Neurocytol, 2003,32(1):79-96
53 Bidkhori G, Narimani Z, Hosseini Ashtiani S, *et al*. Reconstruction of an integrated genome-scale co-expression network reveals key modules involved in lung adenocarcinoma. PLoS ONE, 2013,8(7):e67552
54 Park JI. Growth arrest signalling of the Raf/MEK/ERK pathway in cancer. Front Biol (Beijing), 2014,9(2):95-103
55 Giordano G, Febbraro A, Tomaselli E, *et al*. Cancer-related CD15/FUT4 overexpression decreases benefit to agents targeting EGFR or VEGF acting as a novel RAF-MEK-ERK kinase downstream regulator in metastatic colorectal cancer. J Exp Clin Cancer Res, 2015,34:108
56 Wang N, Li Y, Li Z, *et al*. IRS-1 targets TAZ to inhibit adipogenesis of rat bone marrow mesenchymal stem cells through PI3K-Akt and MEK-ERK pathways. Eur J Pharmacol, 2019,849:11-21

(Received May. 5, 2022; accepted Oct. 18, 2022)